

Prediction of absolute unsaturated hydraulic conductivity - comparison of four different capillary bundle models

Andre Peters^{1*}, Sascha C. Iden¹, and Wolfgang Durner¹

¹Division of Soil Science and Soil Physics, Institute of Geocology, Technische Universität Braunschweig,
5 Germany

Correspondence to: Andre Peters (a.peters@tu-braunschweig.de)

Abstract. To model water, solute, and energy transport in porous media, it is essential to have accurate information about the soil hydraulic properties (SHP), i.e. the water retention curve (WRC) and the soil hydraulic conductivity curve (HCC). It is important to have reliable data to parameterize these models, but equally critical is the selection of appropriate SHP models. While various expressions for the WRC are frequently compared, the capillary conductivity model proposed by Mualem (1976a) is widely used but rarely compared to alternatives. The objective of this study was to compare four different capillary bundle models in terms of their ability to accurately predict the HCC without scaling the conductivity function by a measured conductivity value. The four capillary bundle models include two simple models proposed by Burdine (1953) and Alexander and Skaggs (1986), which assume a bundle of parallel capillaries with tortuous flow paths, and two more sophisticated models based on statistical cut-and-random-rejoin approaches, namely those proposed by Childs and Collis-George (1950) and the aforementioned model of Mualem (1976a). To examine how the choice of the WRC parametrization affects the adequacy of different capillary bundle models, we utilized four different capillary saturation models in combination with each of the conductivity prediction models, resulting in 16 SHP model schemes. All schemes were calibrated using 12 carefully selected datasets that provided water retention and hydraulic conductivity data over a wide saturation range. Subsequently, the calibrated models were tested and rated by their ability to predict the hydraulic conductivity of 23 independent datasets of soils with varying textures. The statistical cut-and-random-rejoin models, particularly the Mualem (1976a) model, outperformed the simpler capillary bundle models in terms of predictive accuracy. This was independent of the specific WRC model used. Our findings suggest that the widespread use of the Mualem model is justified.

1. Introduction

Representing the soil hydraulic properties in functional form is useful for simulation of water, energy, and solute transport in the vadose zone. The most established models for the WRC (e.g., van Genuchten, 1980, or Kosugi, 1996) and the HCC (e.g., Burdine, 1953, or Mualem, 1976a) account for water storage and flow in capillaries but neglect water flow and adsorption in films and corners. The latter effects become, however, dominant if the soils get dry. Therefore, more recent models extend these SHP models (e.g., Tuller and Or, 2001; Peters and Durner, 2008; Lebeau and Konrad, 2010; Zhang, 2011; Peters, 2013; Weber et al., 2019; de Rooij et al., 2021; de Rooij, 2022) to account for these processes. Over the last 10 years, a variety of SHP models have been proposed, see e.g., Li et al. (2023) and the references therein. In the very dry range, vapor flow becomes the dominant transport process. Under isothermal conditions, diffusion of water vapor can be included by an equivalent hydraulic conductivity (Peters, 2013; Iden et al., 2021a; 2021b).

The current models used to predict the HCC, which include both capillary and non-capillary components, do not predict the absolute hydraulic conductivity, $K(h)$ but require scaling of a relative conductivity function, $K_r(h)$, using measured data. Indeed, both the capillary conductivity and the film and corner conductivity must be scaled in some of these models (Peters, 2013). This approach is unsatisfactory as data in the relevant moisture range may be missing (particularly in the dry range) or unreliable (if saturated conductivity is dominated by soil structure), leading to considerable uncertainties in the HCC. To overcome these shortcomings, Peters et al. (2021) proposed a simple yet physically based prediction scheme for the absolute non-capillary conductivity by combining the physically based models for film conductivity proposed by Lebeau and Konrad (2010) and Tokunaga (2009) with the empirical Peters-Durner-Iden (PDI) model developed by Peters (2013; 2014) and Iden and Durner (2014). In a recent study, Peters et al. (2023) extended the HCC prediction from the WRC to the absolute capillary conductivity component using the Mualem (1976a) capillary bundle model. This allows for a conductivity prediction that covers the entire moisture range from near saturation to oven dryness and overcomes the limitations associated with missing or unreliable conductivity data in the relevant moisture range.

A multitude of models has been proposed to describe capillary conductivity. In this work, we focus on the models that derive the pore-size distribution from the capillary water retention function and use the law of Hagen-Poiseuille and some assumptions about connectivity and tortuosity to predict the hydraulic conductivity, the so-called capillary bundle models. We restrict the analysis to the prominent models of Childs and Collis-George (1950), Burdine (1953), Mualem (1976a), and Alexander and Skaggs (1986). As pointed out by Peters et al. (2023), these

models are traditionally used to predict the relative conductivity (i.e., the shape of the $K(h)$ relationship) from the WRC and scale it with a measured matching point, most often the measured saturated conductivity (K_s). The models of Burdine (1953) and Alexander and Skaggs (1986) assume that the relative conductivity is derived from a simple bundle of continuous tortuous capillaries. To achieve a simple mathematical expression, Alexander and Skaggs (1986) assumed that the tortuosity depends on capillary saturation and pore radius.

Childs and Collis-George (1950) (CCG) proposed a more sophisticated statistical cut-and-random-rejoin model. This model was later enhanced by Mualem (1976a) through the incorporation of a correlation between pore length and pore diameter in the rejoined pore connections. Comprehensive overviews of the different model types can be found in Mualem and Dagan (1978), Mualem (1986), and Assouline and Or (2013). Although these different models are mentioned in numerous publications, most studies use only Mualem's (1976a) model.

Several comparisons of capillary bundle models have been published. Jackson et al. (1965) compared four models, which are all variations and modifications of the original CCG model, and either predicted the absolute hydraulic conductivity or used one matching factor to scale $K_r(h)$. In their work, the predictions overestimated the conductivities drastically, and the CCG version of Millington and Quirk (1961) with a matching factor gave the best results. Jackson (1972) compared the CCG model versions of Millington and Quirk (1961) and Marshall (1958), which differ in the way tortuosity and pore connectivity are accounted for, by predicting $K_r(h)$ and scaling it with the measured K_s as a matching factor. He found that the models either over- or underestimate $K(h)$ and suggested an intermediate value for the tortuosity and pore connectivity term. Van Genuchten and Nielsen (1985) compared the Mualem (1976a) and Burdine (1953) models in terms of predicting $K_r(h)$ and found the Mualem (1976a) model to perform better. Nimmo and Akstin (1988) compared the models of CCG, Purcell (1949) adapted by Gates and Lietz (1950), Burdine (1953), and Mualem and used one measured unsaturated conductivity as a matching factor. They found, by visual inspection, that the model of Mualem outperformed the other models. Kosugi (1999) compared the Burdine and Mualem models to predict $K_r(h)$ with his generalized version of the Mualem and Dagan (1978) model, which was first fitted to the data to obtain the general parameter values. Not surprisingly, his version outperformed the predictive models. Moreover, the Mualem model performed better than the Burdine model. Hoffmann-Riem et al. (1999) fitted also a general version of the Mualem and Dagan (1978) model to data and compared it with the models of Mualem and Burdine. They concluded that a fit of the models to data should be conducted to obtain a good description. Finally, Madi et al. (2018) compared the capillary bundle models of Burdine (1953), Mualem (1976a), and Alexander and Skaggs (1986) in terms of their applicability in predicting $K_r(h)$. They found that the Alexander and Skaggs model strongly overestimated $K(h)$ for most soils,

whereas the performances of the Burdine and Mualem models were superior. None of these studies considered non-capillary conductivity. Moreover, besides the comparison of Jackson et al. (1965), none of the studies conducted a prediction of $K(h)$ without adjusting conductivity parameters.

This study aims to compare capillary-bundle models, including Childs and Collis-George (1950), Burdine (1953),
90 Mualem (1976a), and Alexander and Skaggs (1986), regarding their predictive performance for $K(h)$ within the
PDI model framework outlined by Peters et al. (2023). To assess the impact of different WRC parametrizations on
model performance, we combined four alternative unimodal capillary saturation models with the four conductivity
prediction models, resulting in 16 SHP model combinations. Calibration was conducted using 12 datasets providing
sufficient information on WRC and HCC, followed by performance testing on 23 independent datasets representing
95 different soil textures.

2. Theory

All capillary bundle models use a mathematical formulation of the capillary water retention function to express the effective pore-size distribution of a porous medium. We refer to Mualem and Dagan (1978), Mualem (1986) or Peters et al. (2023) for a thorough discussion and mathematical derivation of the most popular capillary bundle
100 models. In this study, we use the Peters-Durner-Iden (PDI) model system (Peters, 2013; 2014; Iden and Durner, 2014) to describe the WRC and HCC in the complete moisture range, because it accounts for capillary and non-capillary liquid storage and conductivity as well as vapor conductivity in a simple form and has proven its ability to describe SHP data well. A full description of the PDI model system is given in appendix A1. In the following, we only briefly review the capillary-bundle model formulations used in this study.

105 2.1 Tortuosity coefficient in capillary bundle models

A key role in all capillary-bundle models is played by the so-called tortuosity-connectivity correction, which differs between the various models proposed. It accounts in a lumped manner for all effects that distinguish a porous medium from a bundle of parallel tubes. The term tortuosity itself describes the effect that the path length for single parcels of water, l_p , is longer than the direct projection distance l through the soil. Compared to water flow in
110 straight capillaries, this leads to a reduction in the local conductivity caused by (i) a longer local flow path and (ii) a locally smaller hydraulic gradient (Bear, 1972). The reduction of the effective hydraulic conductivity is expressed by a tortuosity coefficient τ [-]:

$$\tau = \left(\frac{l}{l_p}\right)^2 \quad (1)$$

Note that τ is not a constant, but a function of water content, since path length increases with decreasing water content. Furthermore, $\tau \neq 1$ at full water saturation because the flow path is always tortuous.

115 2.2 Relative capillary hydraulic conductivity prediction by capillary bundle models

Capillary bundle models are typically used to predict the relative capillary conductivity, $K_{rc}(h)$ [$L T^{-1}$] and need to be scaled by a scaling parameter, usually the saturated capillary conductivity, K_{sc} [$L T^{-1}$], leading to:

$$K_c(h) = K_{sc} K_{rc}(h) \quad (2)$$

where K_c [$L T^{-1}$] is the absolute capillary conductivity. Note that in the original works of Burdine (1953), Childs and Collis-George (1950), Mualem (1976a) and Alexander and Skaggs (1986), K_{sc} is identical to the total saturated
120 conductivity K_s [$L T^{-1}$], whereas in the PDI scheme, K_s is given by the sum of saturated capillary and noncapillary conductivities (see appendix A1).

Burdine model (Bur)

Burdine (1953) suggested that relative conductivity of porous media is described simply by the conductivity of a bundle of parallel tortuous capillaries of different size, where the tortuosity is inversely related to the capillary
125 saturation leading to:

$$K_{rc} = S_c^2 \frac{\int_0^{S_c} h^{-2} d\tilde{S}_c}{\int_0^1 h^{-2} d\tilde{S}_c} \quad (3)$$

where \tilde{S}_c is the dummy variable of integration. The expression S_c^2 describes the dependence of the tortuosity correction on saturation S_c [-] ($0 < S_c < 1$).

Alexander and Skaggs (AS)

Alexander and Skaggs (1986) used a similar expression as Burdine (1953) but assumed that the tortuosity depends
130 on the saturation and the pore radius by $l_p/l = C\sqrt{r/S_c}$ where C [$L^{-1/2}$] is a constant, which was not further specified, yielding:

$$K_{rc} = S_c \frac{\int_0^{S_c} h^{-1} d\tilde{S}_c}{\int_0^1 h^{-1} d\tilde{S}_c} \quad (4)$$

Note that the tortuosity correction is not only given by S_c but is based on the assumption $l_p/l = C\sqrt{r/S_c}$.

Childs and Collis-George (CGG)

Childs and Collis-George (1950) developed a statistical cut-and-random-rejoin-model, which was further modified
 135 by Millington and Quirk (1961) and Kunze et al. (1968), and can be expressed in a general integral form by
 (Mualem, 1976a):

$$K_{rc} = S_c^\lambda \frac{\int_0^{S_c} (S_c - \vartheta) h^{-2} d\vartheta}{\int_0^1 (1 - \vartheta) h^{-2} d\vartheta} \quad (5)$$

where ϑ is a variable of integration, which represents the capillary saturation as function of h between the boundary
 limits, i.e. 0 and S_c (Mualem and Dagan, 1978). The tortuosity parameter λ [-] is either 1 (Kunze et al., 1968) or
 4/3 (Millington and Quirk, 1961).

140 Mualem (Mual)

Mualem (1976a) used the general approach of CCG and assumed that the length of a pore is directly proportional
 to its radius, which leads to:

$$K_{rc} = S_c^\lambda \left[\frac{\int_0^{S_c} h^{-1} d\tilde{S}_c}{\int_0^1 h^{-1} d\tilde{S}_c} \right]^2 \quad (6)$$

Applying his model to a variety of data, Mualem found empirically that $\lambda \approx 0.5$.

We may classify these four models into two groups, (i) relatively simple capillary bundle models (Bur, AS), which
 145 assume a bundle of parallel capillaries with tortuous flow paths, and (ii) two more sophisticated statistical cut-and-
 random-rejoin-models (CCG, Mual). Note that the tortuosity correction S_c^λ in these models becomes unity at
 saturation because it describes only the relative tortuosity reduction in drying soils.

2.3 Absolute capillary hydraulic conductivity prediction

Peters et al. (2023) (in the remainder ‘‘P23’’) reformulated the capillary bundle model of Mualem (1976a) to predict
 150 absolute capillary conductivity. In a first step, they expressed the saturation-dependent absolute tortuosity

coefficient τ [-] as the product of a relative tortuosity coefficient τ_r [-] ($0 < \tau_r < 1$) and a saturated tortuosity coefficient (τ_s) [-]:

$$\tau(S_c) = \tau_s \tau_r(S_c). \quad (7)$$

If we use Mualem's original expression for the relative tortuosity coefficient, $\tau_r = S_c^{0.5}$, the absolute conductivity prediction model reads (P23):

$$K_c = \beta \tau_s S_c^{0.5} (\theta_s - \theta_r)^2 \left[\int_0^{S_c} h^{-1} dS_c \right]^2 \quad (8)$$

155 where θ_s [$\text{m}^3 \text{ m}^{-3}$] and θ_r [$\text{m}^3 \text{ m}^{-3}$] are the saturated and maximum adsorbed water contents, respectively. The coefficient $\beta = \sigma^2 / (2\eta\rho g)$ [$\text{L}^3 \text{ T}^{-1}$] lumps all physical constants originating from the laws of Hagen-Poiseuille and Young-Laplace, where ρ [M L^{-3}] is the fluid density, g [L T^{-2}] is gravitational acceleration, η [$\text{M L}^{-1} \text{ T}^{-1}$] is dynamic viscosity and σ [M T^{-2}] is the surface tension between the fluid and gas phases. The values of the physical constants used in this study are summarized in table 1. If we use SI units, $\beta = 3.04 \times 10^{-4} \text{ m}^3 \text{ s}^{-1}$. If we use cm as
 160 length unit and d as time unit, $\beta = 2.62 \times 10^7 \text{ cm}^3 \text{ d}^{-1}$. P23 discussed that τ_s does not only describe the saturated tortuosity in the strict sense (Eq. (1)), but lumps also other soil- and fluid-related factors, i.e. the surface roughness of pore walls, effects of non-circular capillaries, dead-end pores, and deviations of surface tension and viscosity of the fluid from those of pure water. Moreover, the chosen capillary bundle model will not represent the pore distribution and connectivity in an ideal way.

165

Table 1: Physical constants at 20°C used in this study.

Parameter	Definition	Unit	value
σ	Surface tension between fluid and gas phase	N m^{-1}	0.0725
η	Dynamic viscosity of the bulk liquid	N s m^{-2}	8.90×10^{-4}
ρ	Density of pure water at 298.15 K	kg m^{-3}	997.04
g	Gravitational acceleration constant	m s^{-2}	9.81

In essence, τ_s is the scaling parameter for the conductivity function in Eq. (8), as opposed to K_s in traditional prediction models. The underlying hypothesis is that the saturated tortuosity coefficient, unlike K_s , is subject to

only moderate variations in soil and sample characteristics. Using the Fredlund and Xing (1994) saturation model within the PDI system as model for capillary water retention and Eq. (8) for the capillary conductivity function, P23 confirmed this hypothesis and found that τ_s has an average value of about 0.095 for soils differing greatly in their texture.

In P23, the analysis was restricted to the Mual model. In this paper, we apply the approach of P23 also to CCG, Bur, and AS. This leads to the expressions listed in table 2. For the complete derivation of the models Bur, CCG, and Mual, we refer to Mualem and Dagan (1978). For the AS model, the relative tortuosity is not solely given by S_c (see 2.2). Therefore, τ_s is given by $1/C^2$, has the dimension L, and the parameter β is replaced by $\beta' = \sigma/4\eta$ (see appendix A2). With the values in table 1, $\beta' = 20.4 \text{ m s}^{-1}$, resp. $\beta' = 1.76 \times 10^8 \text{ cm d}^{-1}$.

Table 2: Summary of the four prediction models for capillary hydraulic conductivity.

Name	prediction model for K_c	
Mual	$\beta \tau_s S_c^{0.5} (\theta_s - \theta_r)^2 \left[\int_0^{S_c} h^{-1} dS_c \right]^2$	(9)
CCG	$2\beta \tau_s S_c^{4/3} (\theta_s - \theta_r) \int_0^{S_c} (S_c - \vartheta) h^{-2} d\vartheta$	(10)
Bur	$\beta \tau_s S_c^2 (\theta_s - \theta_r) \int_0^{S_c} h^{-2} dS_c$	(11)
AS	$\beta' \tau_s S_c (\theta_s - \theta_r) \int_0^{S_c} h^{-1} dS_c$	(12)

180

3. Materials and Methods

3.1 Model combinations

To represent the complete SHP, we combined the four different capillary bundle models (table 2) for the conductivity prediction with four basic capillary saturation functions (table 3) within the PDI model system, leading to a total of 16 SHP model combinations. The chosen saturation functions are the van Genuchten (1980) saturation function with (vGc) and without (vGmn) the constraint $m = 1 - 1/n$ (table 3), the Kosugi (1996) saturation function (Kos), and the saturation function of Fredlund and Xing (1994) (FX). We selected these functions because they are among the most commonly used unimodal saturation functions in the field of soil physics and geotechnics. In each of the 16 model combinations, the relative tortuosity parameter λ was set to the original proposed values of $\lambda = 4/3$ for the CCG model (Version of Millington and Quirk, 1961), $\lambda = 2.0$ for the Burdine model, $\lambda = 0.5$ for the Mualem model, and $\lambda = 1.0$ for the AS model.

Table 3: Summary of the four capillary saturation functions. The parameters α , n , m , σ_{kos} , and h_m are shape parameters and e is the Euler number. These functions are scaled to the value range between 0 and 1 within the PDI scheme by Eq. (A.2).

Name	Basic capillary saturation function $S_c(h)$	
Kos	$\frac{1}{2} \operatorname{erfc} \left[\frac{\ln \left(\frac{h}{h_m} \right)}{\sqrt{2} \sigma_{kos}} \right]$	(13)
vGc	$\left(\frac{1}{1 + (\alpha h)^n} \right)^{1-1/n}$	(94)
vGmn	$\left(\frac{1}{1 + (\alpha h)^n} \right)^m$	(15)
FX	$\left(\frac{1}{\ln[e + (\alpha h)^n]} \right)^m$	(16)

195

Capillary bundle models can lead to unrealistic drops in the HCC close to water saturation if the pore-size distribution underlying the WRC is wide (e.g., Vogel et al., 2000, Ippisch et al., 2006, Madi et al., 2018). To prevent such unrealistic decreases of $K(h)$, we applied the ‘‘hclip’’ approach of Iden et al. (2015). In this approach, an

upper bound for the pore size is assumed in the conductivity calculation by the pore-bundle models. This is equivalent to limiting the suction to a minimum value h_{crit} , i.e. setting $h = \min(h, h_{\text{crit}})$ in Eqs. (9) to (12). For the Mual model, this leads to:

$$K_c = \beta \tau_s S_c^{0.5} (\theta_s - \theta_r)^2 \left[\int_0^{S_c} (\min(h, h_{\text{crit}}))^{-1} dS_c \right]^2 \quad (17)$$

Following Jarvis (2007) we assumed the maximum equivalent pore diameter of 0.5 mm, corresponding to $h_{\text{crit}} = 0.06$ m. Within the context of the proposed absolute prediction scheme, the "clipped" models are identical to the "unclipped" models for suctions exceeding h_{crit} .

Since there exist no analytical solutions for several of the model combinations with respect to the capillary conductivity functions, we solved the integrals of the capillary conductivity functions (table 2) by means of numerical integration using the trapezoidal method.

210 3.2 Calibration of τ_s for each model

For each of the 16 model combinations, a model-specific τ_s was determined by fitting the WRC and HCC models to measured data. The adjustable parameters were all WRC parameters and τ_s . For the non-capillary conductivity, which becomes important in the medium to dry range, where film and corner flow is dominant, we used the prediction model of Peters et al. (2021). To obtain reliable estimates for τ_s , (i) data for the water retention function and (ii) hydraulic conductivity data in the wet range, but not at saturation, are required in high quality. We used the same 12 data sets that were already used by P23. The data encompass a wide variety of soil textures, from a pure sand to a clay loam. Details about the soils are given in the original literature and are summarized in table 4.

Models were fitted to the data by nonlinear, weighted least squares regression. The objective function was

$$\phi(\mathbf{b}) = w_\theta \sum_{i=1}^{n_\theta} [\theta_i - \tilde{\theta}_i(\mathbf{b})]^2 + w_K \sum_{i=1}^{n_K} [\log_{10}(K_i) - \log_{10}(\tilde{K}_i(\mathbf{b}))]^2 \quad (18)$$

220 Here, θ_i and $\tilde{\theta}_i$ are the measured and modeled water contents, K_i and \tilde{K}_i are measured and modeled hydraulic conductivities, n_θ and n_K are the respective number of data points, $w_\theta = 10000$ and $w_K = 16$ are weights for the two data groups (Peters, 2011) and \mathbf{b} is the vector of unknown model parameters. The SCE-UA algorithm (Duan et al., 1992), was applied to minimize the objective function. Details can be found in P23. Model performance was

225 quantified by the root mean squared errors (RMSE) of volumetric water content (WRC) and common log of $K(h)$ (HCC).

Table 4: SHP data used for model fitting.

Data set ID	Data set name in original publication	Source	Texture Class
Cal 1	Rehovot Sand	Mualem (1976b)	Sand
Cal 2	Gilat Loam		Loam
Cal 3	Pachapa Fine Sandy Clay (PFSC)		Sandy Clay
Cal 4	-	Pachepsky et al. (1984)	Sandy Loam
Cal 5	-		Silt Loam
Cal 6	-		Clay Loam
Cal 7	GG first sample	Sarkar et al. (2019)	Silt Loam
Cal 8	GG second sample		Silt Loam
Cal 9	JKI first sample		Loamy Sand
Cal 10	JKI second sample		Loamy Sand
Cal 11	SAU first sample		Sand
Cal 12	SAU second sample		Sand

3.3 Testing the predictive performance of the models

230 The performance of the various HCC prediction schemes was tested by comparing purely predicted HCC functions with measured conductivity data. For this test, we used the same 23 validation data sets as P23. Details about the data is given in table 5. The test data comprise again a broad range of different texture classes. The PDI retention model with the four basic saturation functions given in table 3 was fitted to the water retention data, and the conductivity functions were predicted with the model-specific values of τ_s as determined through calibration.

Table 5: Data sets used to test the conductivity predictions.

Data set ID	Data set name in original publication	Source	Texture Class
-------------	---------------------------------------	--------	---------------

Test 1*	-	Peters et al. (2023)	Silt Loam
Test 2*	-		Sandy Loam
Test 3*	-		Sandy Loam
Test 4	-		Sand
Test 5	-		Sandy Loam
Test 6	-		Loamy Sand
Test 7	-		Loamy Sand
Test 8	-		Sand
Test 9	-		Sand
Test 10	-		Loamy Sand
Test 11	-		Loamy Sand
Test 12**	coarse sand	Peters et al. (2019)	Sand
Test 13	sand 1	Schelle et al. (2013)	Sand
Test 14	silt loam 1		Silt Loam
Test 15	sand 2a		Sand
Test 16*	silt loam 2		Silt Loam
Test 17*	sand 2b		Sand
Test 18*	silt		Silt
Test 19*	GG	Kirste et al. (2019)	Silt Loam
Test 20*	JKI		Sandy Loam
Test 21*	SAU		Sand
Test 22	HEB		Silt Loam
Test 23	SEL		Silty Clay Loam

* samples taken at same sites but different years as some of the calibration data (Cal7 to Cal 12)

235 ** disturbed sample

4. Results

4.1 Model-specific τ_s for the 16 model combinations

Figure 1 shows 4 out of the 12 calibration data sets and the corresponding fitted SHP. We chose the FX-PDI model as saturation function for illustration since P23 found that it performed best in describing the retention data. The fitted HCC represent the 4 capillary bundle models tested. Overall, the differences between different WRC models and the associated conductivity curves are small (see supplementary material). We limit Fig. 1 to four soils in order to keep the presentation concise; the corresponding graphs for all soils and all 16 model combinations are given in the supplementary material.

The goodness-of-fit for the 4 models is quantified by the $RMSE_{\theta}$ and $RMSE_{\log K}$ (Fig.2). The cut-and-random-rejoin models proposed by Mualem and CCG give rather small RMSE for the retention as well as the conductivity curves, whereas the conceptually simpler models of Burdine and AS perform less well. Specifically, the AS model could often describe the conductivity data adequately only at the expense of a poorer fit of the WRC data. Figure A1 shows the $RMSE_{\theta}$ and $RMSE_{\log K}$ boxplots for all 16 model combinations, revealing that the specific findings for the FX basic function can be generalized.

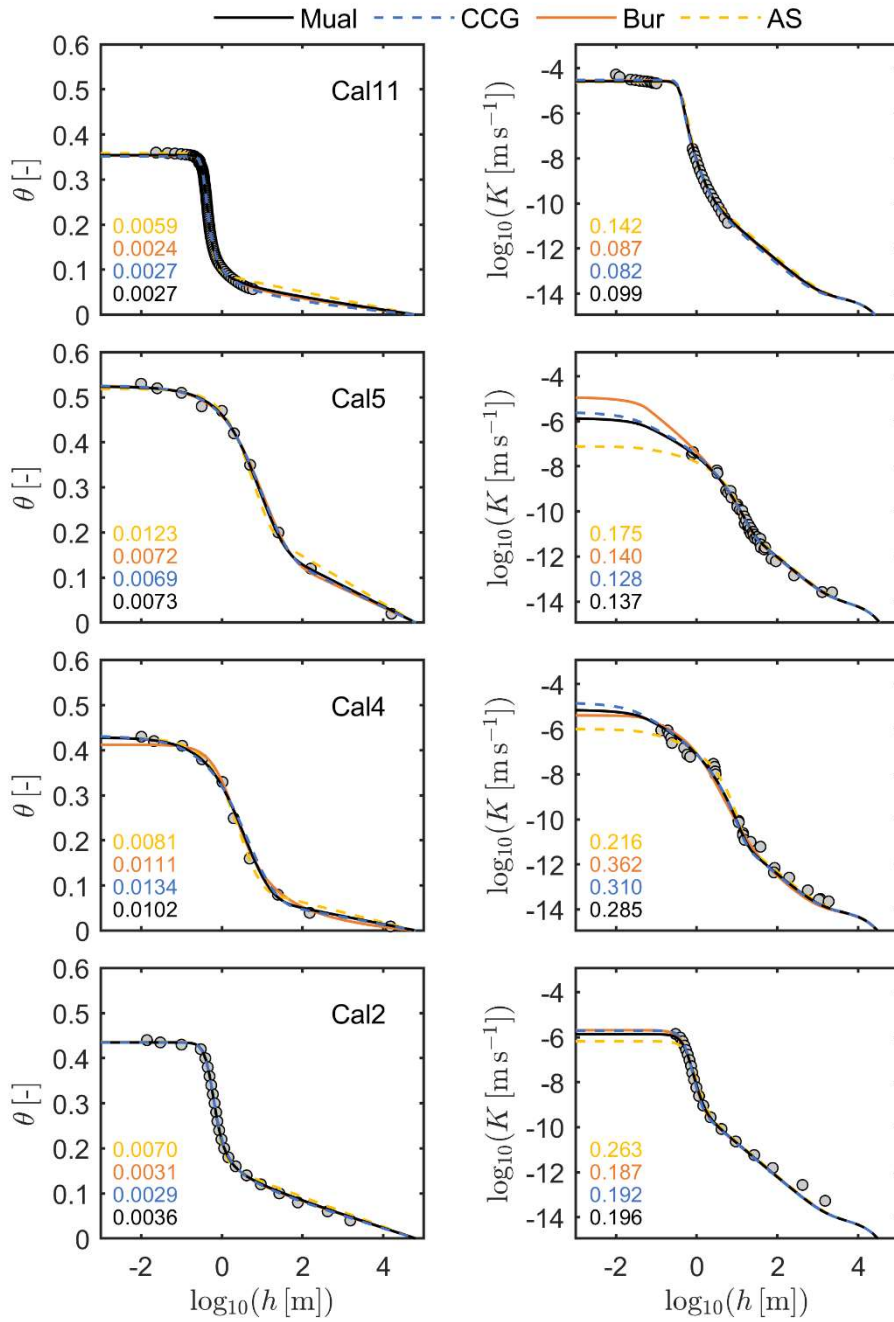


Figure 1: Plots of 4 of the 12 calibration data sets together with the fitted SHP functions. The FX-PDI model was used for WRC and four capillary bundle models were used for the HCC. The estimated parameters were the five parameters of the FX-PDI and the saturated tortuosity coefficient τ_s . The numbers in the subplots indicate RMSE_θ and RMSE_{logK} values for the four models.

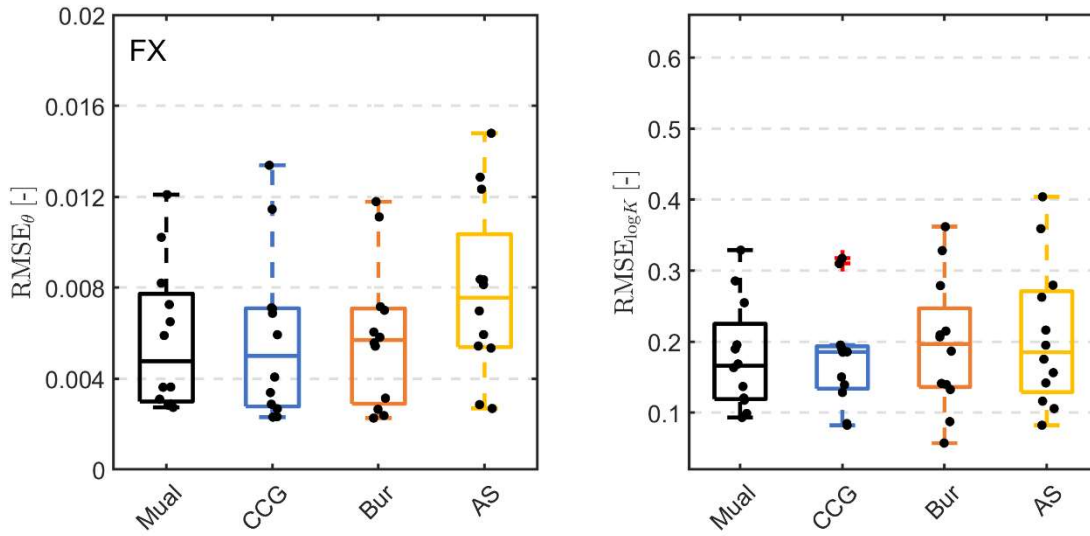


Figure 2: Distributions of $RMSE_{\theta}$ and $RMSE_{\log K}$ when fitting the FX-PDI retention model in combination with the four capillary conductivity functions listed in table 2 to the 12 calibration data sets. Black dots indicate single realizations. The red cross indicates an outlier, defined by the Matlab® default settings as 1.5 times the inter quartile range away from the top or bottom of the box (<https://de.mathworks.com/help/matlab/ref/boxchart.html>).

260

Figure 3 shows that the different conductivity prediction models give different optimal values for the saturated tortuosity coefficient, τ_s . This is in accordance with the discussion of the nature of τ_s in Peters et al. (2023) who acknowledge that the notion of a universally applicable saturated pore tortuosity is untenable. Rather, it must be seen as a general parameter in the context of the specific conceptualization of a capillary bundle model. The median values for τ_s are 0.095 for the Mualem model (as in P23), 0.27 for CCG, 0.014 for Burdine, and 7.8×10^{-5} for the AS model if the WRC is parameterized by the FX-PDI function. Note that τ_s has the unit [m] for the AS model, whereas it is dimensionless for the other models. The values vary within a range of approximately 1.5 orders of magnitude for the Mual and CCG models, slightly less than 2 orders of magnitude for the Bur model, and more than 2 orders of magnitude for the AS model. The systematic differences of τ_s between the capillary bundle models can be attributed to the differing conceptual approaches implicit to these models, as the physical parameters of fluid properties are consistent, and the functional representation of the effective pore-size distribution was the same. We note that models based on Mual and CCG result in quite similar τ_s values whereas those of the Bur model are a bit smaller. The AS model gives completely different values. Actually, the interpretation of τ_s in the AS model is difficult since part of the tortuosity is accounted for in the capillary model. Fig. A2 shows the distributions of the τ_s values for all 16 model combinations. The medians of the estimated values for τ_s are summarized in table 6.

270

275

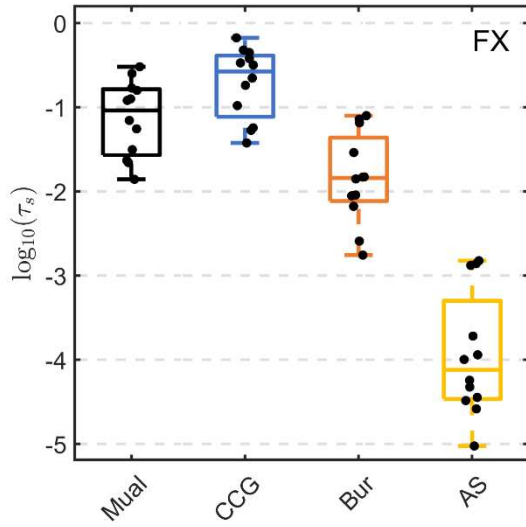


Figure 3: Distribution of optimal τ_s values obtained by fitting the four conductivity prediction models with the FX-PDI retention model to the 12 calibration data sets given in table 4. Black dots indicate single realizations.

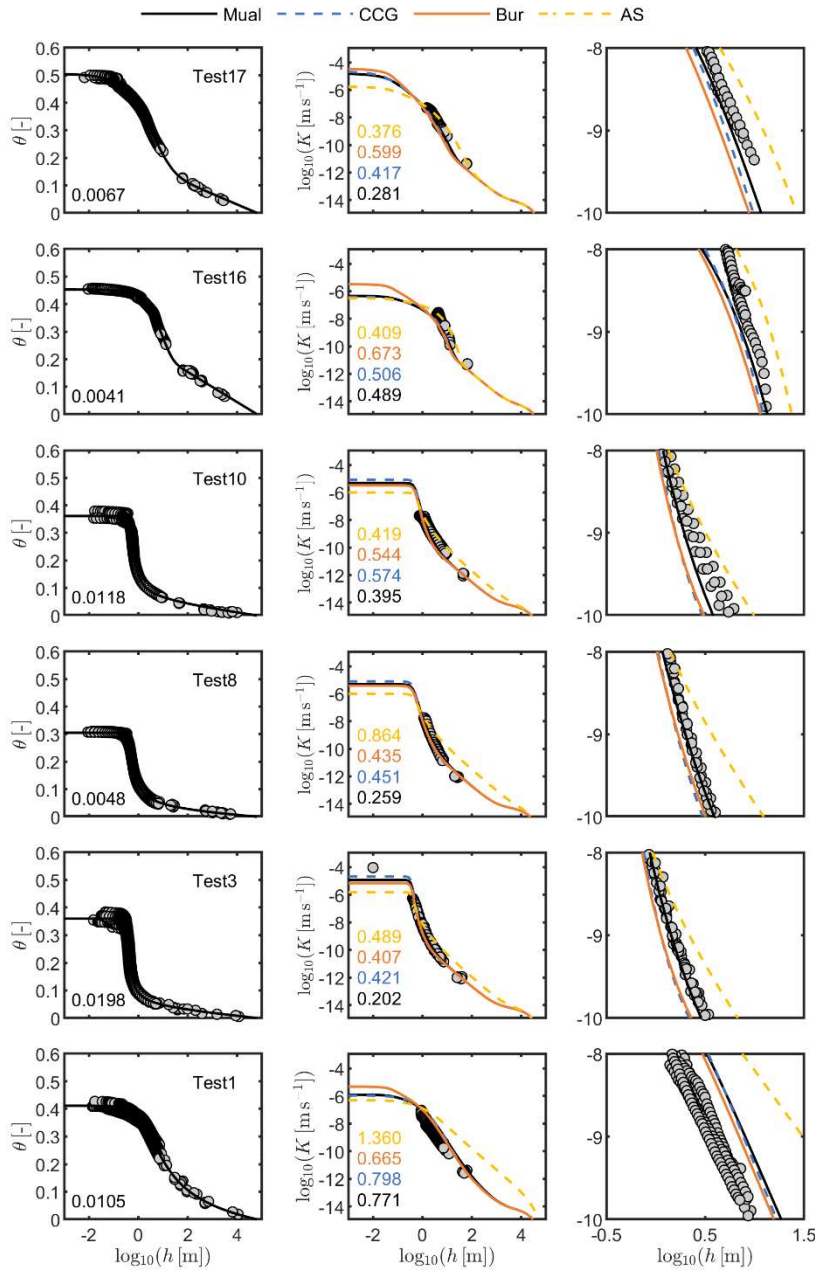
Table 6: Estimated values (median) of τ_s for all 16 model combinations.

	Mual	CCG	Bur	AS [m]
Kos	0.084	0.230	0.011	7.7E-05
vGc	0.061	0.182	0.011	8.0E-05
vGmn	0.093	0.272	0.015	7.8E-05
FX	0.095	0.268	0.014	7.8E-05

280 4.2 Conductivity prediction accuracy by the different capillary bundle models

Fitting the retention models to the water retention data and using the values of τ_s obtained from the calibration (table 6), we predicted the complete hydraulic conductivity functions for the 23 validation data sets and the 16 model combinations. Figure 4 shows the predicted functions and the data exemplarily for 6 out of the 23 data sets, again for the FX basic saturation model. With the exception of the AS model, the purely predicted conductivity

285 curves agree remarkably well with the measured independent data. The curves for all data sets are given in the supplementary material.



290 **Figure 4:** Measured data (dots), fitted retention functions (left) and predicted (not fitted) conductivity functions (center: complete curves; right: zoomed curves). Shown are 6 randomly selected soils out of 23 validation data sets. Numbers in the subplots indicate the $RMSE_{\theta}$ for the FX-PDI WRC model and the $RMSE_{\log K}$ values for the AS, Bur, CCG and Mual conductivity models, from top to bottom.

Figure 5 shows the accuracy of the conductivity predictions again for the FX-PDI retention model, expressed by boxplots of the $RMSE_{\log K}$ and the mean error ($ME_{\log K}$). The distributions for all 16 model combinations are shown in Fig. A3. The median $RMSE_{\log K}$ in Fig. 5 is 0.40 for the Mual model, which yields the best prediction of all 16 model schemes. For the CCG model the median $RMSE_{\log K}$ is 0.42, for the Bur model it is 0.44. For the AS model it is worst with a value of 0.66. Furthermore, the AS model leads to the largest variation in the prediction accuracy.

For all 16 model combinations (Fig. A3), the Mual model performed best for any of the investigated retention models. Table 7 lists the median $RMSE_{\log K}$ for all 16 model combinations. With the exception of the prediction that is based on the FX-PDI model, the median accuracy of the AS is as good or even better than the CCG and the Bur model. However, the AS prediction accuracy shows for any WRC model a large spread of $RMSE_{\log K}$ with values up to 1.4 (Fig. 5; Fig. A3), which corresponds to a mismatch by a factor 25 in the K values. Contrary, the Mual model performs not only well with respect to the median values but yields also the lowest spread for the $RMSE_{\log K}$ for any of the saturation functions, in other words it is the most robust. Figure 5 (right) and Fig. A3 indicate furthermore that only the combination of the FX capillary saturation function with the Mual capillary bundle model leads to unbiased results. Summarizing the above findings, the preferred model combination is the basic FX saturation model with Mualem's capillary conductivity model and $\tau_s = 0.095$. These results support the findings of van Genuchten and Nielsen (1985), Nimmo and Akstin (1988), and Kosugi (1999), who also found the Mualem model to perform best in their model comparisons.

The somewhat non-robust performance of the AS model, also found by Madi et al. (2018), can be explained by its assumption regarding tortuosity. We analyze this assumption in more detail in appendix A4.

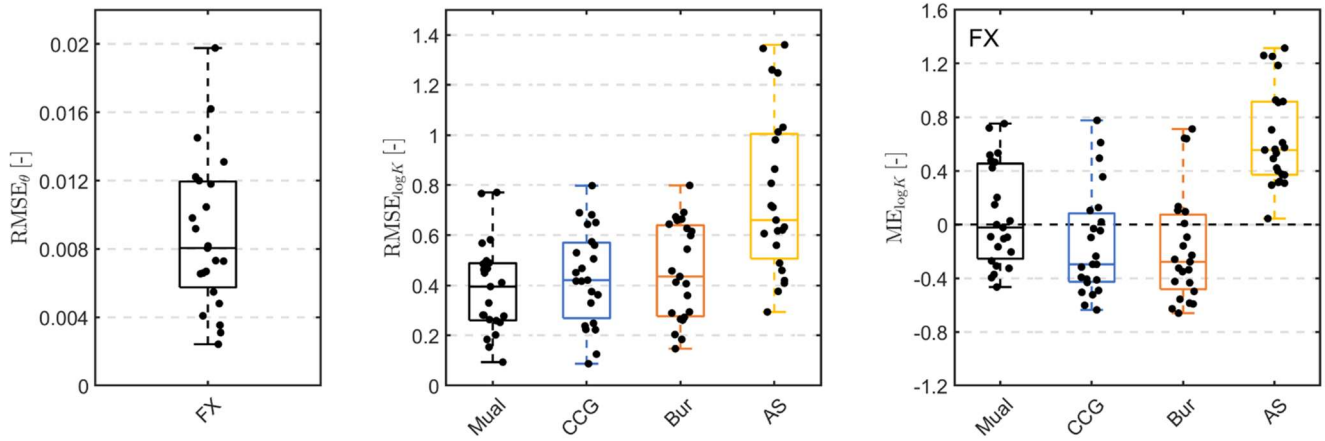


Figure 5: Left: $RMSE_{\theta}$ of the fitted PDI-FX retention model for the 23 test data sets. Center and right: $RMSE_{\log K}$ and mean errors of the predicted absolute conductivities by the four models listed in Table 2. Black dots indicate single realizations.

315

Table 7: Median of $RMSE_{\log K}$ for all model combinations.

	Mual	CCG	Bur	AS
Kos	0.69	0.79	0.81	0.74
vGc	0.64	0.73	0.78	0.66
vGmn	0.48	0.60	0.65	0.45
FX	0.40	0.42	0.44	0.66

4.3 Behavior of the capillary bundle models in the wet range

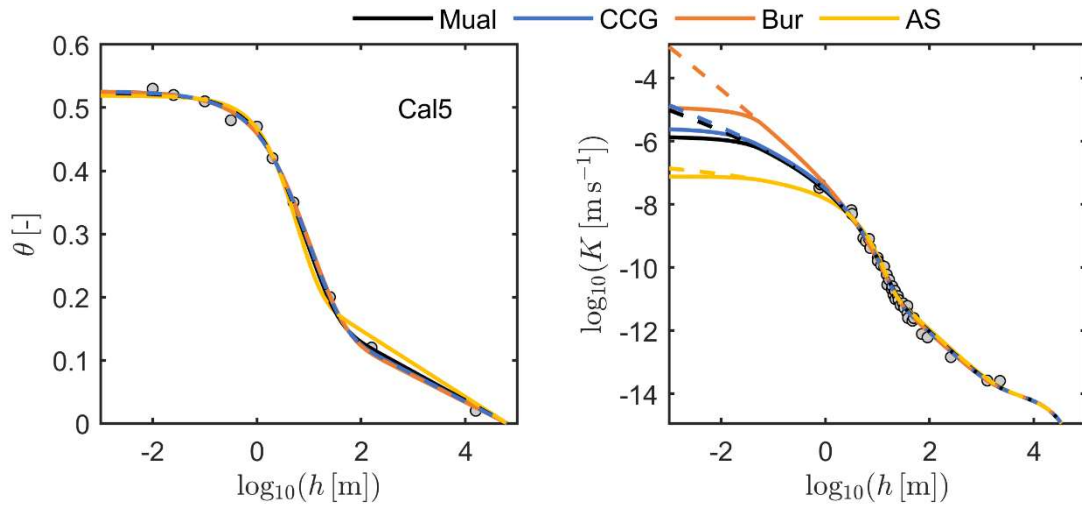
320 In the very wet moisture range, even tiny changes in the WRC can have a large impact on the HCC. Such small changes at arbitrary small suctions occur in common WRC parameterizations for soils with wide pore-size distributions or for bimodal soils. Durner (1994) concluded accordingly three decades ago that this makes a conductivity prediction based on statistical pore-bundle models in the range close to full saturation virtually impossible. In Fig. 6, we evaluate this effect for the 4 different conductivity prediction models. For illustration, we use the rather fine textured silt loam (calibration data set 5, shown in Fig. 1, too) and show all model fits with and

325 without consideration of a maximum pore-size in the capillary bundle models (“hclip”, Iden et al., 2015), as described in section 3.1.

In all cases, we fitted the retention model parameters and τ_s to the data. The fitted WRC (FX-PDI) lie almost on top of each other (again with a slight difference for the AS model, as discussed in section 4.3). The WRC fits differ slightly for the different model combinations although we used always the same retention model because the
330 retention parameters α , n and m influence the shape of both hydraulic functions, which were simultaneously fitted by minimizing Eq. (18). The four conductivity models fit the given data similarly well, but show a very different behaviour in the wet moisture range, where no data are available. All models with the exception of the AS model show in the “unclipped” version (dashed lines) a strong increase of conductivity in the pressure range close to saturation, from about $h < 0.01$ m. This illustrates the artifact of using capillary bundle-models without limiting
335 the maximum pore size in the integrals used to calculate the conductivity function. In a classic approach where the relative conductivity function is predicted and matched to a measured or assumed value for K_s , the unsaturated conductivity curve would be underestimated markedly. The AS model appears to be least affected by this artifact.

However, even if the change of the HCC close to saturation caused by this artifact is removed by introducing a maximum pore size in the integrals (9) to (12), the four models differ markedly in their predicted shape in the
340 moderately moist region (Fig. 6, "with clipping"; solid lines). The differences between the 4 models reach still almost 2 orders of magnitude and they develop in a suction range where we are still far from unrealistically large pores sizes (recall that in the “hclip curves”, the maximum allowed pore diameter was 0.5 mm, corresponding to a suction of 0.06 m).

The reason for the varying behaviour lies in the distinct pore-bundle models utilized. The Bur model, which
345 assumes that the pore paths are parallel and tortuous, yields the greatest conductivity increase for large pores due to the Hagen-Poiseuille relationship with pore size. In contrast, the CCG and Mual models, which involve cutting and randomly rejoining most of the direct paths, mitigate this effect and exhibit comparable patterns. The AS model leads to the smallest change in hydraulic conductivity in the wet range.



350 **Figure 6:** Fitted retention and conductivity functions with and without “hclip” to calibration set Cal 5. Solid lines: with clipping; dashed lines: without clipping. Basic capillary saturation function is the FX model.

5. Summary and conclusion

In this study, we compared 4 different capillary bundle models in combination with 4 different unimodal capillary saturation models, leading to 16 model combinations, to predict the absolute hydraulic conductivity within the PDI model framework. For each of the 16 model combinations, we determined a model-specific value for the saturated tortuosity coefficient, τ_s , by fitting the models to a calibration data set. Using these general values of τ_s , we then predicted, for independent data sets, all three components of conductivity, namely isothermal vapor, non-capillary, and capillary liquid conductivity, from the WRC without any adjusted parameters, following Peters et al. (2021; 2023).

360 When predicting the HCC from the WRC, a good representation of the water retention function is essential; therefore, the best-performing model schemes were those that used the flexible 3-parameter capillary saturation functions in the WRC model (i.e., the Fredlund and Xing (1994) model and the unconstrained van Genuchten (1980) model with independent parameters m and n).

Among the capillary bundle models, the cut-and-random-rejoin models introduced by Childs and Collis-George (1950) and Mualem (1976a) exhibited the best performance, with the Mualem model performing slightly superior. 365 The Burdine (1953) model was less suited, while the model of Alexander and Skaggs (1986) performed worst. The use of the AS model is, therefore, not recommended due to its unphysical representation of relative tortuosity. Since

the model of Mualem (1976a) is mathematically simpler than the model of Childs and Collis-George (1950), we conclude that its establishment in soil hydrology is justified. The median $RMSE_{\log K}$ was 0.4 for the recommended
370 FX-PDI-Mualem combination. In other words, the median relative error of the predicted K is about a factor of 2.6, which appears fair enough in the light of the expected measurement uncertainties.

It is interesting to note that even when fitted to the data, the various models exhibit distinct behavior near saturation during extrapolation. This can be attributed to differences in their model structures. Specifically, the Burdine model tends to overestimate the conductivity increase caused by the presence of even small amounts of water in large
375 pores, as it directly applies the law of Hagen-Poiseuille to a specific pore diameter derived from the WRC. In contrast, the two cut-and-random-rejoin models result in a much smaller conductivity contribution from water stored in the largest pores due to the random combination of pores of different sizes. The AS model, on the other hand, appears to underestimate the conductivity increase in the wet range.

Our approach estimates the hydraulic conductivity of the soil matrix, excluding the influence of soil structure. It
380 can be useful in situations without available conductivity data. When a measured value of saturated conductivity (K_s) is available, especially for topsoils where soil structure plays a significant role, combining our predicted hydraulic conductivity curve (HCC) with interpolation towards K_s can yield a well-defined conductivity function across the entire moisture range, as discussed in P23. This approach distinguishes between structural and textural effects, ensuring the consistent use of measured SHP information and allowing for the estimation of soil structure
385 formation extent.

Appendix

A 1. The PDI Model System

A 1.1. PDI Water Retention Function

The capillary saturation function S_c [-] and a non-capillary saturation function S_{nc} [-] may be superposed in the
390 form (Peters, 2013; Iden and Durner, 2014):

$$\theta(h) = (\theta_s - \theta_r)S_c + \theta_r S_{nc}, \quad (\text{A.1})$$

in which the first right term describes water stored in capillaries, and the second term water stored in adsorbed water films and pore corners, θ [$\text{m}^3 \text{m}^{-3}$] is the total water content, h [m] is the suction head and θ_s [$\text{m}^3 \text{m}^{-3}$] and θ_r

395 $[\text{m}^3 \text{m}^{-3}]$ are the saturated and maximum adsorbed water contents, respectively. To meet the physical requirement that the capillary saturation function reaches zero at oven dryness, a basic saturation function $\Gamma(h)$ is scaled by (Iden and Durner, 2014):

$$S_c(h) = \frac{\Gamma(h) - \Gamma(h_0)}{1 - \Gamma(h_0)}, \quad (\text{A.2})$$

with h_0 [m] is the suction head at oven dryness, which can be set at $10^{4.8}$ m following Schneider and Goss (2012). $\Gamma(h)$ can be any uni- or multi-modal saturation function such as the unimodal functions of van Genuchten (1980) and Kosugi (1996), or their bimodal versions (Durner, 1994; Romano et al., 2011).

The saturation function for non-capillary water is given by a smoothed piecewise linear function (Iden and Durner, 2014), which is here given in the notation of Peters et al. (2021):

$$S_{nc}(h) = \frac{\ln\left(\frac{h_0}{h}\right) - b \ln\left(1 + \left[\frac{h_a}{h}\right]^{1/b}\right)}{\ln\left(\frac{h_0}{h_a}\right)}, \quad (\text{A.3})$$

in which the parameter h_a [m] reflects the suction head where non-capillary water reaches its saturation (fixed in our study to the suction at which capillary saturation reaches 0.75). The derivation for h_a as a quantile of S_c is given in Peters et al. (2023) and the resulting mathematical expressions are listed below in appendix A.1.3. The parameter h_0 in Equation (A.3) is the suction head where the water content reaches zero, which reflects the suction at oven-dry conditions. $S_{nc}(h)$ increases linearly from zero at oven dryness to its maximum value of 1.0 at h_a , and then remains constant toward saturation. In order to ensure a continuously differentiable water capacity function, $S_{nc}(h)$ must be smoothed around h_a , which is achieved by the smoothing parameter b [-] (Iden and Durner, 2014), given here by:

$$b = b_o \left(1 + 2 \frac{1 - e^{-b_1}}{n^2}\right), \quad (\text{A.4})$$

where $b_o = 0.1 \ln(10)$ and $b_1 = \left(\frac{\theta_r}{\theta_s - \theta_r}\right)^2$.

A 1.2. PDI Hydraulic Conductivity

415 The PDI hydraulic conductivity model is expressed as (Peters et al., 2013):

$$K(h) = K_c + K_{nc} + K_v, \quad (\text{A.5})$$

where K_c [-] [m s^{-1}], K_{nc} [m s^{-1}], and K_v [m s^{-1}] are the conductivities for the capillary, non-capillary and isothermal vapor conductivities respectively. K_{nc} is given by (Peters et al., 2021):

$$K_{nc} = c \theta_m h_a^{-1.5} \left(\frac{h_0}{h_a} \right)^{-1.5(1-S_{nc})}, \quad (\text{A.6})$$

420 in which c is used to account for several physical and geometrical constants and can be either a free fitting parameter to scale K_{nc} or $c = 1.35 \times 10^{-8} \text{ m}^{5/2} \text{ s}^{-1}$. Parameter θ_m [-] is the water content at $h = 10^3 \text{ m}$. We refer to Saito et al. (2006) or Peters (2013) for details regarding the formulation of K_v as a function of the invoked WRC. The conductivity for water flow in capillaries is in this paper described using the 4 pore bundle models summarized in table 2.

425 A 1.3. Calculation of h_a

According to Peters et al. (2023), we set the air entry parameter for the non-capillary parts of the hydraulic functions, h_a to the suction at which capillary saturation reaches 0.75. The expressions for the used capillary saturation functions are summarized in Tab A1.

430 **Table A1:** Mathematical expressions for h_a for the used capillary saturation functions as derived by Peters et al. (2023). The parameter γ is given by $\gamma = \xi(1 - \Gamma_0) + \Gamma_0$, where ξ [-] is the chosen quantile of the capillary saturation for the derivation of h_a (in our case ξ is 0.75).

Name	Mathematical expressions for h_a
Kos	$h_m e^{\sqrt{2} \sigma} \text{erfc}^{-1}(2\gamma)$
vGc and vGmn	$\alpha^{-1} \left[\gamma^{-\frac{1}{m}} - 1 \right]^{1/n}$
FX	$\alpha^{-1} \left(\exp\left(\gamma^{-\frac{1}{m}}\right) - e \right)^{\frac{1}{n}}$

A 2. Derivation of Alexander and Skaggs (1986) model

435 The capillary conductivity functions $K_c(S_c)$ [$L T^{-1}$] given by a slightly modified version of Equation (4) in Alexander and Skaggs (1986) is:

$$K_c = (\theta_s - \theta_r) \frac{\rho g}{8\eta} \int_0^{S_c} r^2 \left(\frac{l}{l_p}\right)^2 d\tilde{S}_c \quad (A7)$$

where θ_s [-] and θ_r [-] are the saturated and residual water contents, S_c [-] is the capillary saturation, ρ [$kg m^{-3}$] is the fluid density, g [$m s^{-2}$] is gravitational acceleration, η [$N s m^{-2}$] is dynamic viscosity, r [m] is the radius of the capillary, which is assumed to have a circular cross-section, l [L] is the direct projection distance through the soil, l_p [m] path length for single water molecules and \tilde{S}_c is the dummy variable of integration. The quotient l_p/l is the path elongation due to tortuosity. Note that for consistency, we use the maximum water filled capillaries, $\theta_s - \theta_r$, instead of porosity and the potential in the Hagen-Poiseuille law is here given in length units.

445 Applying the Young-Laplace relation, $r = \kappa/h$ with $\kappa = 2\sigma/\rho g$, where σ [$N m^{-2}$] is the surface tension between the fluid and gas phases, and h [m] the suction, leads to:

$$K_c = (\theta_s - \theta_r) \frac{\rho g}{8\eta} \int_0^{S_c} \frac{\kappa^2}{h^2} \left(\frac{l}{l_p}\right)^2 d\tilde{S}_c \quad (A8)$$

Alexander and Skaggs (1986) assumed that the path elongation due to tortuosity, i.e. l_p/l depends on the saturation and the pore radius by

$$l_p/l = C\sqrt{r/S_c} \quad (A9)$$

450 where C [$m^{-1/2}$] is a constant, which is not further specified. Using the Young-Laplace relation leads to:

$$l_p/l = C\sqrt{\kappa/(hS_c)} \quad (A10)$$

Inserting Eq. (4) into Eq. (2) gives:

$$K_c = (\theta_s - \theta_r) \frac{\rho g}{8\eta} \int_0^{S_c} \frac{\kappa^2}{h^2} \frac{h\tilde{S}_c}{c^2\kappa} d\tilde{S}_c = (\theta_s - \theta_r) \frac{\rho g}{8\eta} \int_0^{S_c} \frac{\kappa}{h} \frac{\tilde{S}_c}{c^2} d\tilde{S}_c \quad (A11)$$

Substituting $\kappa = 2\sigma/\rho g$ yields:

$$455 \quad K_c = (\theta_s - \theta_r) \frac{\sigma}{4\eta} \frac{1}{c^2} \int_0^{S_c} \frac{S_c}{h} d\tilde{S}_c \quad (A12)$$

Since h is a function of S_c , Eq. (6) can be solved using partial integration, which leads to:

$$K_c = (\theta_s - \theta_r) \frac{\sigma}{4\eta} \frac{1}{c^2} \left\{ S_c \int_0^{S_c} \frac{1}{h} d\tilde{S}_c - \int_0^{S_c} \int_0^{S_c} \frac{1}{h} d\tilde{S}_c d\tilde{S}_c \right\} \quad (\text{A13})$$

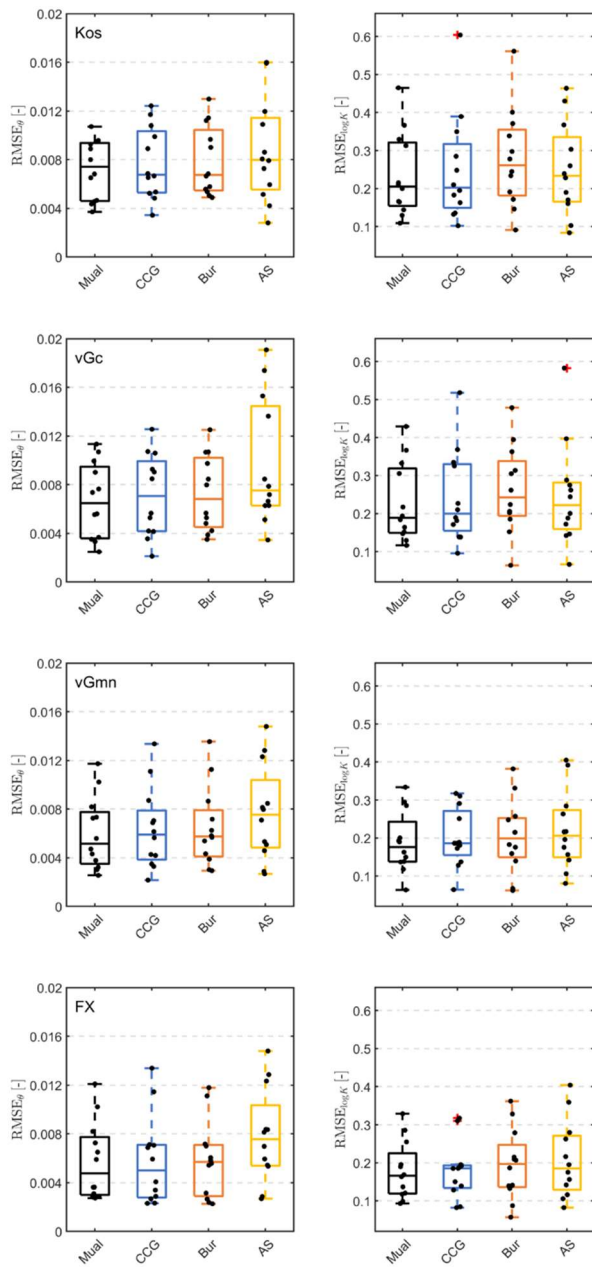
Alexander and Skaggs neglected the last term in the curly brackets, which leads to:

$$K_c = (\theta_s - \theta_r) \frac{\sigma}{4\eta} \frac{1}{c^2} S_c \int_0^{S_c} \frac{1}{h} d\tilde{S}_c \quad (\text{A14})$$

460 In our notation, τ_s is given by $1/C^2$ and has the unit m, and the parameter β is replaced by $\beta' = \sigma/4\eta$, which finally leads to:

$$K_c = \beta' \tau_s S_c (\theta_s - \theta_r) \int_0^{S_c} \frac{1}{h} d\tilde{S}_c \quad (\text{A15})$$

A 3. Results for all model combinations



465

Figure A1: Distributions of $RMSE_0$ and $RMSE_{logK}$ when fitting the 4 retention model in combination with the four capillary conductivity functions listed in tables 2 and 3 to the 12 calibration data sets. 1st row: Kos as basic saturation function; 2nd row: vGc as basic saturation function; 3rd row: vGmn as basic saturation function; 4th row: FX as basic saturation function. Black dots indicate single realizations. The red crosses indicate outliers, defined by the Matlab® default settings as 1.5 times the inter quartile range away from the top or bottom of the box (<https://de.mathworks.com/help/matlab/ref/boxchart.html>).

470

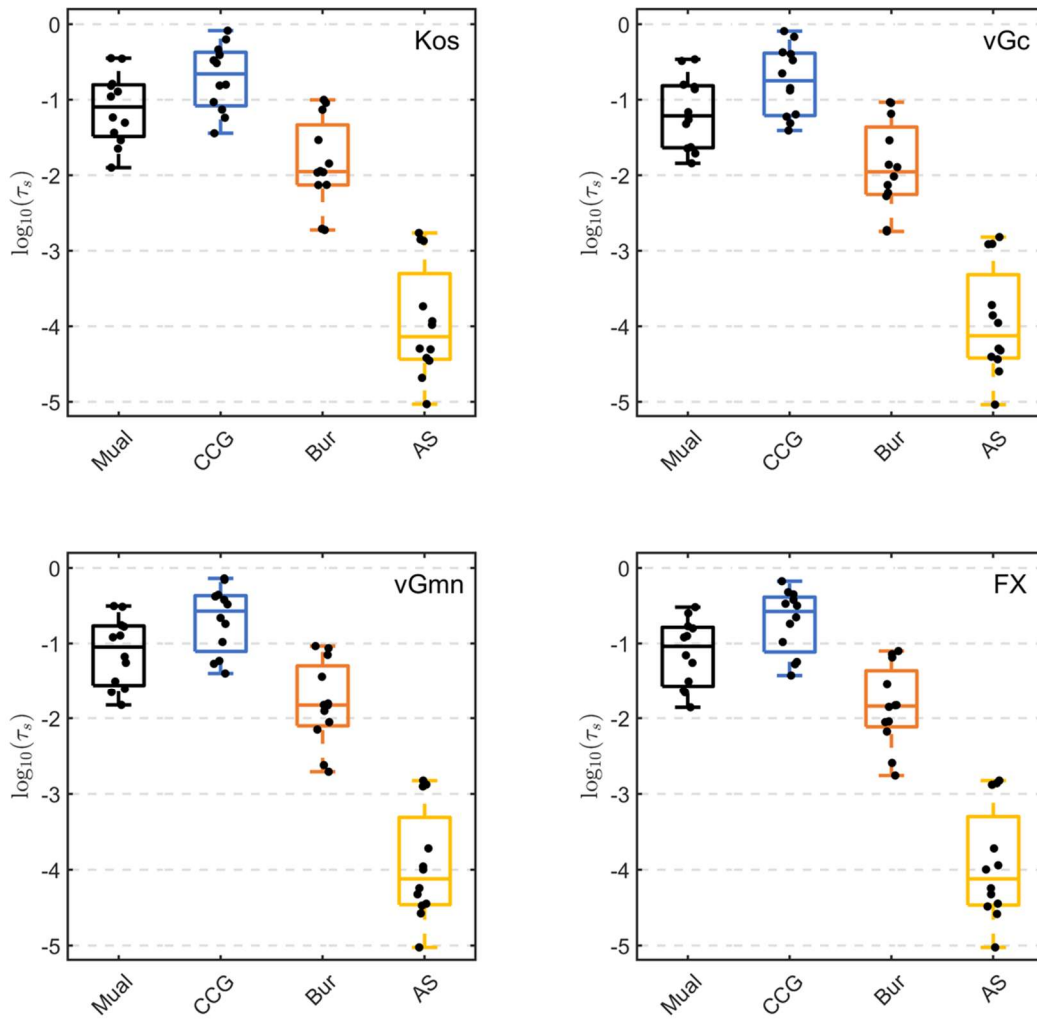


Figure A2: Distribution of fitted τ_s values for the 4 different capillary bundle models and the 4 basic capillary saturation functions fitted to the 12 data sets (see Fig. 6) given in table 4. Black dots indicate single realizations. Top, left: Kos as basic saturation function; Top, right: vGc as basic saturation function; Bottom, left: vGmn as basic saturation function; Bottom, right: FX as basic saturation function.

475

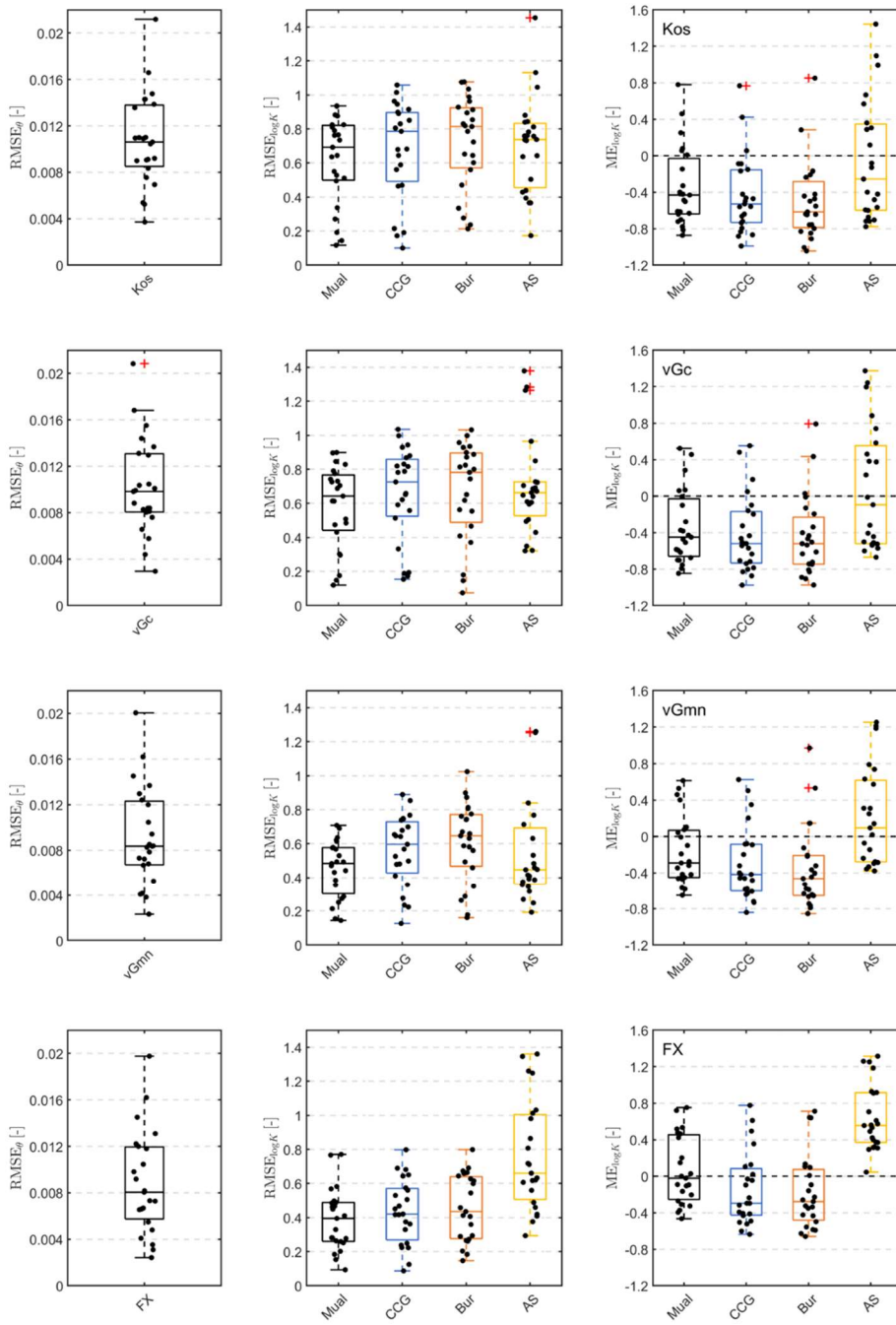
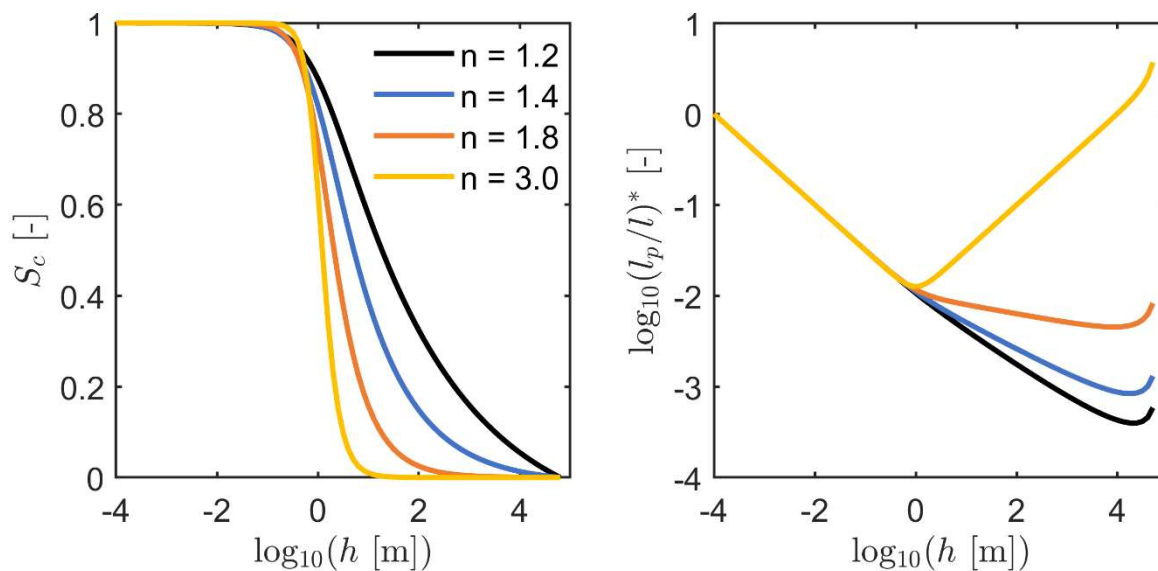


Figure A3: Left: $RMSE_{\theta}$ of the fitted PDI retention models for the 23 test data sets. Center and right: $RMSE_{\log k}$ and mean errors of the predicted absolute conductivities for all 4 different capillary bundle models and the 4 basic capillary saturation functions listed in tables 2 and 3. Black dots indicate single realizations. 1st row: Kos as basic saturation function; 2nd row: vGc as basic saturation function; 3rd row: vGmn as basic saturation function; 4th row: FX as basic saturation function. The red crosses indicate outliers, defined by the Matlab® default

A 4. Analyzing the tortuosity assumption of Alexander and Skaggs (1986)

485 Physically, the path elongation due to tortuosity l_p/l should strictly increase with decreasing saturation. In the AS model it is assumed to follow $l_p/l = C\sqrt{r/S_c}$. Figure A4 visualizes the relationship between tortuosity and pressure head for four different capillary saturation functions, which reflect differently wide pore-size distributions. The path elongation l_p/l , plotted as relative function $(l_p/l)^*$, decreases with increasing h (decreasing saturation) which is unphysical. The only exception is found for the very narrow pore-size distribution in the range beyond the
 490 air-entry point. When fitting simultaneously the WRC and HCC, this behavior of the AS conceptual model is counteracted by a worse fit of the retention data (see Figs. 1 and 2). In a pure prediction, where only the retention model is fitted, this can lead to a bad performance of the conductivity prediction. Similar to our results, Madi et al. (2018), who used the measured saturated conductivity for scaling, found that the AS model severely overestimates the unsaturated conductivity for most soils.



495

Figure A4: Scaled tortuosity correction used by AS conductivity prediction model for soils with different pore-size distributions. Left: Capillary saturation functions using the vGc saturation function with $\alpha = 1.0 \text{ m}^{-1}$ and n varying from 1.2 to 3.0. Right: associated scaled tortuosity correction $l_p/l = C\sqrt{r/S_c}$. Since we are only interested in the general shape of the function, we scaled l_p/l by assuming $C = 1$ and dividing it by its value at $h = 10^{-4} \text{ m}$.

500

Data availability: The calibration data sets Cal 1 to Cal 6 cannot be provided due to copyright restrictions (Cal 1 to Cal 3: Mualem (1976b); Cal 4 to Cal 6: Pachepsky et al. (1984)). The other six calibration data sets and all test data sets are given in the supplemental material S2.

Acknowledgments: This study was financially supported by the Deutsche Forschungsgemeinschaft (DFG grant PE 1912/4-1).

Author contributions: Conceptualization: AP; model implementation and analysis: AP; draft preparation and discussions: AP, SCI, and WD.

Competing interests: The contact author has declared that none of the authors has any competing interests.

510 **References**

Alexander, L., and Skaggs, R. W.: Predicting unsaturated hydraulic conductivity from the soil water characteristic. *Transactions of the ASAE*, 29(1), 176-184, doi: 10.13031/2013.30123, 1986.

Assouline, S. and Or, D.: Conceptual and parametric representation of soil hydraulic properties: A review, *Vadose Zone J.*, 12, 1–20, <https://doi.org/10.2136/vzj2013.07.0121>, 2013.

515 Bear, J.: *Dynamics of Fluids in Porous Media*, Elsevier, New York, ISBN 0486131807, 1972.

Burdine, N.: Relative permeability calculations from pore size distribution data, *J. Petrol. Technol.*, 5, 71–78, 1953.

Childs, E. C. and Collis-George, N.: The permeability of porous materials, *Proc. R. Soc. Lon. Ser.-A*, 201, 392–405, 1950.

de Rooij, G. H.: A sigmoidal soil water retention curve without asymptote that is robust when dry-range data are
520 unreliable. *Hydrology and Earth System Sciences*, 26(22), 5849-5858, 2022.

de Rooij, G. H., Mai, J., and Madi, R.: Sigmoidal water retention function with improved behaviour in dry and wet soils, *Hydrol. Earth Syst. Sci.*, 25, 983–1007, <https://doi.org/10.5194/hess-25-983-2021>, 2021.

Duan, Q., Sorooshian, S., and Gupta, V.: Effective and efficient global optimization for conceptual rainfall-runoff models, *Water Resour. Res.*, 28, 1015–1031, 1992.

- 525 Durner, W.: Hydraulic conductivity estimation for soils with heterogeneous pore structure, *Water Resour. Res.*, 30, 211–222, <https://doi.org/10.1029/93WR02676>, 1994.
- Fredlund, D. G. and Xing, A. Q.: Equations for the soil water characteristic curve, *Can. Geotech. J.*, 31, 521–532, <https://doi.org/10.1139/t94-061>, 1994.
- Gates, J. I., and Lietz, W. T.: Relative permeabilities of California cores by the capillary-pressure method. In
530 *Drilling and production practice*, p. 285-298, Am. Petrol. Inst., New York, 1950.
- Hoffmann-Riem, H., van Genuchten, M. Th., and Flühler, H.: General model for the hydraulic conductivity of unsaturated soils, in *Proceedings of the International Workshop on Characterization and Measurement of the Hydraulic Properties of Unsaturated Porous Media*, edited by M. Th. van Genuchten, F. J. Leij, and L. Wu, pp. 31–42, Univ. of California, Riverside, California, 1999.
- 535 Iden, S. and Durner, W.: Comment on “Simple consistent models for water retention and hydraulic conductivity in the complete moisture range” by A. Peters, *Water Resour. Res.*, 50, 7530–7534, <https://doi.org/10.1002/2014WR015937>, 2014.
- Iden, S. C., Peters, A., and Durner, W.: Improving prediction of hydraulic conductivity by constraining capillary bundle models to a maximum pore size, *Adv. Water Resour.*, 85, 86–92, 2015.
- 540 Iden, S. C., Blöcher, J. R., Diamantopoulos, E., and Durner, W.: Capillary, Film, and Vapor Flow in Transient Bare Soil Evaporation (1): Identifiability Analysis of Hydraulic Conductivity in the Medium to Dry Moisture Range. *Water Resources Research*, 57(5), e2020WR028513. <https://doi.org/10.1029/2020WR028513>, 2021a.
- Iden, S. C., Diamantopoulos, E., and Durner, W.: Capillary, Film, and Vapor Flow in Transient Bare Soil Evaporation (2): Experimental Identification of Hydraulic Conductivity in the Medium to Dry Moisture Range.
545 *Water Resources Research*, 57(5), e2020WR028514. <https://doi.org/10.1029/2020WR028514>, 2021b.
- Ippisch, O., Vogel, H.-J., and Bastian, P.: Validity limits for the van Genuchten–Mualem model and implications for parameter estimation and numerical simulation, *Adv. Water Resour.*, 29, 1780–1789, 2006.
- Jackson, R. D.: On the calculation of hydraulic conductivity. *Soil Sci. Soc. Am. J.*, 36(2), 380-382, 1972.
- Jackson, R. D., Reginato, R. J., and Van Bavel, C. H. M.: Comparison of measured and calculated hydraulic
550 conductivities of unsaturated soils. *Water Resour. Res.*, 1(3), 375-380, 1965.

- Jarvis, N. J.: A review of non-equilibrium water flow and solute transport in soil macropores: Principles, controlling factors and consequences for water quality, *Eur. J. Soil. Sci.*, 58, 523–546, 2007.
- Kirste, B., Iden, S. C., and Durner, W.: Determination of the soil water retention curve around the wilting point: Optimized protocol for the dewpoint method. *Soil Science Society of America Journal*, 83(2), 288-299, 2019.
- 555 Kosugi, K.: Lognormal distribution model for unsaturated soil hydraulic properties, *Water Resour. Res.*, 32, 2697–2703, 1996.
- Kosugi, K.: General model for unsaturated hydraulic conductivity for soils with lognormal pore-size distribution. *Soil Sci. Soc. Am. J.*, 63, 270-277, 1999.
- Kunze, R. J., Uehara, G., and Graham, K.: Factors important in the calculation of hydraulic conductivity, *Soil Sci. Soc. Am. J.*, 32, 760–765, 1968.
- 560 Lebeau, M. and Konrad, J.-M.: A new capillary and thin film flow model for predicting the hydraulic conductivity of unsaturated porous media, *Water Resour. Res.*, 46, W12554, <https://doi.org/10.1029/2010WR009092>, 2010.
- Madi, R., de Rooij, G. H., Mielenz, H., and Mai, J.: Parametric soil water retention models: a critical evaluation of expressions for the full moisture range, *Hydrol. Earth Syst. Sci.*, 22, 1193–1219, [https://doi.org/10.5194/hess-22-](https://doi.org/10.5194/hess-22-1193-2018)
- 565 1193-2018, 2018.
- Li, P., Zha, Y., Zuo, B., and Zhang, Y.: A family of soil water retention models based on sigmoid functions. *Water Resources Research*, 59(3), e2022WR033160, 2023.
- Marshall, T. J.: A relation between permeability and size distribution of pores. *Journal of soil science*, 9(1), 1-8, 1958.
- 570 Millington, R. J. and Quirk, J. P.: Permeability of porous solids, *T. Faraday Soc.*, 57, 1200–1207, 1961.
- Mualem, Y.: A new model for predicting the hydraulic conductivity of unsaturated porous media, *Water Resour. Res.*, 12, 513–522, 1976a.
- Mualem, Y.: A catalog of the hydraulic properties of unsaturated soils (Tech. Rep), Technion – Israel Institute of Technology, 1976b.
- 575 Mualem, Y.: Hydraulic conductivity of unsaturated soils: Prediction and formulas, *Methods of Soil Analysis: Part 1 Physical and Mineralogical Methods*, 5, 799–822, <https://doi.org/10.2136/sssabookser5.1.2ed.c31>, 1986.

- Mualem, Y., and Dagan, G.: Hydraulic conductivity of soils: Unified approach to the statistical models. *Soil Science Society of America Journal*, 42(3), 392-395, <https://doi.org/10.2136/sssaj1978.03615995004200030003x>, 1978.
- 580 Nimmo, J.R., and Akstin, K.C.: Hydraulic conductivity of a sandy soil at low water content after compaction by various methods. *Soil Sci. Soc. Am. J.*, 52(2), 303-310, 1988.
- Pachepsky, Y., Scherbakov, R., Varallyay, G., and Rajkai, K.: On obtaining soil hydraulic conductivity curves from water retention curves, *Pochvovedenie*, 10, 60–72, 1984 (in Russian).
- Peters, A.: Simple consistent models for water retention and hydraulic conductivity in the complete moisture range, 585 *Water Resour. Res.*, 49, 6765–6780, <https://doi.org/10.1002/wrcr.20548>, 2013.
- Peters, A.: Reply to comment by S. Iden and W. Durner on “Simple consistent models for water retention and hydraulic conductivity in the complete moisture range”, *Water Resour. Res.*, 50, 7535–7539, <https://doi.org/10.1002/2014WR016107>, 2014.
- Peters, A. and Durner, W.: A simple model for describing hydraulic conductivity in unsaturated porous media 590 accounting for film and capillary flow, *Water Resour. Res.*, 44, W11417, <https://doi.org/10.1029/2008WR007136>, 2008.
- Peters, A., Durner, W., and Wessolek, G.: Consistent parameter constraints for soil hydraulic functions, *Adv. Water Resour.*, 34, 1352–1365, 2011.
- Peters, A., Iden, S. C., and Durner, W.: Local Solute Sinks and Sources Cause Erroneous Dispersion Fluxes in 595 Transport Simulations with the Convection–Dispersion Equation, *Vadose Zone J.*, 18, 190064, <https://doi.org/10.2136/vzj2019.06.0064>, 2019.
- Peters, A., Hohenbrink, T. L., Iden, S. C., and Durner, W.: A simple model to predict hydraulic conductivity in medium to dry soil from the water retention curve, *Water Resour. Res.*, 57, e2020WR029211, <https://doi.org/10.1029/2020WR029211>, 2021.
- 600 Peters, A., Hohenbrink, T. L., Iden, S. C., van Genuchten, M. Th., and Durner, W.: Prediction of the absolute hydraulic conductivity function from soil water retention data, *Hydrol. Earth Syst. Sci.*, 27, 1565–1582, <https://doi.org/10.5194/hess-27-1565-2023>, 2023.

- Purcell, W. R.: Capillary pressures-their measurement using mercury and the calculation of permeability therefrom. *Journal of Petroleum Technology*, 1(02), 39-48, <https://doi.org/10.2118/949039-G>, 1949.
- 605 Romano, N., Nasta, P., Severino, G., and Hopmans, J. W.: Using Bimodal Lognormal Functions to Describe Soil Hydraulic Properties, *Soil Sci. Soc. Am. J.*, 75, 468–480, <https://doi.org/10.2136/sssaj2010.0084>, 2011.
- Saito, H., Šimunek, J., and Mohanty, B. P.: Numerical analysis of coupled water, vapor, and heat transport in the vadose zone, *Vadose Zone J.*, 5, 784–800, 2006.
- Sarkar, S., Germer, K., Maity, R., and Durner, W.: Measuring near-saturated hydraulic conductivity of soils by quasi unit-gradient percolation – 2. Application of the methodology, *J. Plant Nutr. Soil Sc.*, 182, 535–540, <https://doi.org/10.1002/jpln.201800383>, 2019.
- 610 Schelle, H., Heise, L., Jänicke, K., and Durner, W.: Water retention characteristics of soils over the whole moisture range: A comparison of laboratory methods, *Eur. J. Soil. Sci.*, 64, 814–821, 2013.
- Schneider, M. and Goss, K.-U.: Prediction of the water sorption isotherm in air dry soils, *Geoderma*, 170, 64–69, <https://doi.org/10.1016/j.geoderma.2011.10.008>, 2012.
- 615 Tuller, M. and Or, D.: Hydraulic conductivity of variably saturated porous media: Film and corner flow in angular pore space, *Water Resour. Res.*, 37, 1257–1276, <https://doi.org/10.1029/2000WR900328>, 2001.
- Tokunaga, T. K.: Hydraulic properties of adsorbed water films in unsaturated porous media, *Water Resour. Res.*, 45, W06415, <https://doi.org/10.1029/2009WR007734>, 2009.
- 620 van Genuchten, M. Th.: A closed-form equation for predicting the hydraulic conductivity of unsaturated soils, *Soil Sci. Soc. Am. J.*, 44, 892–898, 1980.
- van Genuchten, M. Th., and Nielsen, D. R.: On describing and predicting the hydraulic properties of unsaturated soils. *Annales Geophysicae*, 3(5), 615-628, 1985.
- Vogel, T., Van Genuchten, M. T., and Cislerova, M.: Effect of the shape of the soil hydraulic functions near saturation on variably-saturated flow predictions, *Adv. Water Resour.*, 24, 133–144, 2000.
- 625 Weber, T. K., Durner, W., Streck, T., and Diamantopoulos, E.: A modular framework for modeling unsaturated soil hydraulic properties over the full moisture range. *Water Resources Research*, 55(6), 4994-5011, 2019.

Zhang, Z. F.: Soil water retention and relative permeability for conditions from oven-dry to full saturation, *Vadose Zone J.*, 10, 1299–1308, <https://doi.org/10.2136/vzj2011.0019>, 2011.